

Modeling DNA beacons at the mesoscopic scale

Jalal Errami¹, Michel Peyrard¹, and Nikos Theodorakopoulos^{2,3}

¹ Laboratoire de Physique, ENS-Lyon, 46 allée d'Italie, 69364 Lyon Cedex 07, France

² Theoretical and Physical Chemistry Institute, National Hellenic Research Foundation, Vas. Constantinou 48, 11635 Athens, Greece

³ Fachbereich Physik der Universität Konstanz, Fach M 686, 78457 Konstanz, Germany

October 26, 2018

Abstract. We report model calculations on DNA single strands which describe the equilibrium dynamics and kinetics of hairpin formation and melting. Modeling is at the level of single bases. Strand rigidity is described in terms of simple polymer models; alternative calculations performed using the freely rotating chain and the discrete Kratky-Porod models are reported. Stem formation is modeled according to the Peyrard-Bishop-Dauxois Hamiltonian. The kinetics of opening and closing is described in terms of a diffusion-controlled motion in an effective free energy landscape. Melting profiles, dependence of melting temperature on loop length, and kinetic time scales are in semiquantitative agreement with experimental data obtained from fluorescent DNA beacons forming poly(T) loops. Variation in strand rigidity is not sufficient to account for the large activation enthalpy of closing and the strong loop length dependence observed in hairpins forming poly(A) loops. Implications for modeling single strands of DNA or RNA are discussed.

PACS. 87.15.He Dynamics and conformational changes – 87.15.Aa Theory and modeling; computer simulation – 87.14.Gg DNA, RNA – 36.20.Ey Conformation (statistics and dynamics)

1 Introduction

DNA beacons are made of short single strands of DNA with terminal regions consisting of complementary base sequences. As a result the two end-regions can self-assemble in a short DNA double helix, called the stem, while the remaining central part of the strand forms a loop. In this closed configuration, the single strand has the shape of a hairpin. Such hairpin conformations are present in the secondary structure of long single strands of DNA or RNA. A short single strand of DNA which can form a hairpin becomes a so-called “DNA beacon” when one of its ends is attached to a fluorophore while the second end is attached to a quencher. When the fluorophore and the quencher are within a few Angströms of each other, the fluorescence is suppressed due to direct energy transfer from the fluorophore to the quencher. Consequently in a closed hairpin configuration the beacon is not fluorescent, whereas in the open configuration it becomes fluorescent. This property leads to many interesting applications for molecular beacons in biology or physics.

Biological applications use the possible assembly of a portion of the single strand which forms the loop with another DNA strand which is complementary to the loop’s sequence. The assembly of the single strand of the loop with another strand to make a double helix is only possible when the hairpin is open because double-stranded

DNA is very rigid. Therefore, when the assembly occurs, the fluorescent signal is restored [1]. This technique provides very sensitive probes of the sequences which are complementary to the loop. Using this idea, it has been suggested that DNA beacons could be used in vivo to detect the single stranded RNA which is synthesized during the transcription of genes. This could allow the recognition of cancer cells by targeting some genes which are heavily transcribed in those cells [2,3].

Physical applications exploit the high reproducibility of the hairpins’ self-assembly process which makes it possible to build molecular memories read by detecting the fluorescence [4] or devices capable of performing molecular computation [5].

Understanding the DNA hairpin self-assembly process at the mesoscopic scale is possible because molecular beacons allow accurate monitoring of the opening and closing steps. The “melting profile” of the stem, induced by heating, can be recorded accurately versus temperature and the autocorrelation function of the fluorescence can be used to extract the kinetics of the opening/closing fluctuations. Measurements have been made [6] for different loop lengths and different bases in the loop. They provide a complete set of data which can be compared to the results of a theoretical analysis in order to determine the basic mechanisms controlling the properties of DNA hairpins. This is the primary aim of the study presented

here. It should be noted however that our results, because of their strong sensitivity to the properties of the loop, turn out to have implications which extend beyond the properties of hairpins as such. The detailed comparison of experimental data with the results of various loop models enhances our ability to model single strands of DNA and RNA.

2 The model

The closing of a DNA hairpin has some similarity with the folding of a protein in the sense that it is an evolution from a random chain to a geometrical shape which is stabilized by weak bonds established between some of its components, here the bases of the stem. The full process is quite complex because it involves the precise positioning of a large number of atoms in space to form the strands of the stem. However one may reasonably argue that, in order to understand experimental observations such as the fluctuations of a beacon, one does not need to know all the details of the process. A simple view is to consider the DNA strand as a polymer chain. Then it should be possible to combine known models for the stem with a polymer model for the loop. This has been done in an approach that uses the simplest possible model for the stem [7], an Ising model in which the bases are either closed or open, and a semiflexible polymer model for the loop. This approach gave interesting results, in particular concerning the estimation of the persistence length of single-stranded DNA. However it has the drawback that the description of the stem is very rough and relies on empirical parameters, such as the entropy change involved in the closing of two bases, which cannot be justified within the model and have to be fitted. Moreover, as the Ising model of the stem ignores all geometrical parameters, such as the distance between the bases linked to the loop, the matching between the models of the stem and the loop has to be crude. A further aspect which is not satisfactory in such an approach is that it uses two different models for the stem and the loop while both belong to the same DNA single strand, and should be described in the same framework. This is what we are doing in the present study. It should of course be clear that the pairing of bases in the stem leads to additional phenomena which do not occur in the loop and must be taken into account in order to complete the model. Last, but by no means least, we would like to argue that a model with continuous degrees of freedom is more apt to describe the end-to-end distance, which is a natural ‘‘reaction coordinate’’ measured by the fluorescence signal.

A schematic picture of our hairpin model is shown in Fig. 1. It consists of a stem of M base pairs and a loop with L segments, i.e. $L - 1$ bases so that the single strand which forms the hairpin has a total of $2M + L - 1$ bases or $N = 2M + L - 2$ segments. This single strand can be described by different polymer models. The dependence of our results on the particulars of the polymer model will be discussed in Sec. 5. For the moment, let us consider only one of them as the basic model of our study, the

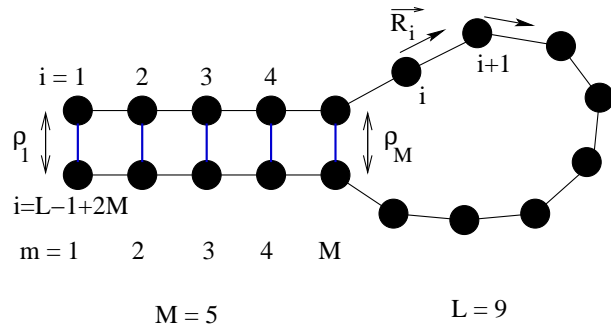


Fig. 1. A schematic picture of the model to define some notations. The hairpin is made of a stem of M base pairs and a loop of L segments, i.e. $L - 1$ bases. The bases along the strand are labeled by an index i ranging from 1 to $L - 1 + 2M$. The variables ρ_m represent the distances between the bases forming base pairs m in the stem. The *stretching* of the base pair distance is denoted by y_m so that $\rho_m = y_m + d$, where d is the equilibrium distance between the bases in a DNA double helix.

Kratky-Porod (KP) [8] model, also known as the wormlike chain (WLC) in its continuum version [12]; for DNA hairpins which have short loops and a very short persistence length the original discrete version is more appropriate. The Kratky-Porod model considers the chain of bases as made of rigid segments of length ℓ . The orientation of a segment in three-dimensional space is defined by a vector \mathbf{R}_i of unit length, lying along segment i , as shown in Fig. 1. Therefore the end-to-end distance of this chain, labeled ρ_1 in Fig. 1 is

$$\rho_1 = \left| \ell \sum_{i=1}^N \mathbf{R}_i \right|. \quad (1)$$

The energy of the KP model is

$$E_1(N) = -\epsilon \ell^2 \sum_{i=1}^{N-1} (\mathbf{R}_i \cdot \mathbf{R}_{i+1} - 1), \quad (2)$$

where $\epsilon \ell^2$ measures the energy that is necessary to bend the polymer at a joint, i.e. it is a parameter that measures the rigidity of the strand.

To complete the description of the hairpin we must also add the interactions which may take place within the stem when base pairing occurs. We use an approach based on the PBD model for DNA melting [9,10] by adding to the polymer model the energy contribution

$$\begin{aligned} E_2(M) = & D \sum_{m=1}^M \left\{ \left[\exp(-\alpha y_m) - 1 \right]^2 - 1 \right\} \\ & + \frac{1}{2} K \sum_{m=2}^M \exp[-\zeta(y_m + y_{m-1})] (y_m - y_{m-1})^2 \\ \equiv & \sum_{m=1}^M V(y_m) + \sum_{m=2}^M W(y_m, y_{m-1}), \end{aligned} \quad (3)$$

where D, α, K, ζ are constant parameters and $y_m = \rho_m - d$ denotes the deviation of the distance ρ_m between two bases in pair m from its equilibrium value, d , in the double helix. In other words y_m is the stretching of the m^{th} base pair in the stem, and is a function of the vectors \mathbf{R}_i which define the geometrical shape of the strand. The potential energy of the stem includes Morse potentials $V(y)$ describing the pairing energy between two complementary bases. The Morse potentials describe an effective interaction which includes the attractive contribution of the hydrogen bonds between the complementary bases and the repulsion coming from the charged phosphate groups on the strands. The other important energy terms in the stem are the stacking interactions between consecutive bases, described by the nonlinear potential $W(y, y')$. In fact stacking energies are also present in an implicit form in the polymer model of the strands since the flexibility of a single strand of DNA is affected by the interactions between the bases which are part of the nucleotides. In the stem however the stacking energy increases because of the geometrical constraints of double helix packing. The base pair plateaux are piled on top of each other and interact strongly due to the overlap of their π electrons. If one of the two adjacent pairs is open the double helix packing disappears and the prefactor $\exp[-\zeta(y_m + y_{m-1})]$ vanishes [11]. It is the geometrical constraint which allows us to use the scalar variable y_m to describe the base pair status in the stem. In this geometry the displacement of the bases is essentially orthogonal to the stem axis and therefore the stretching of the individual base pairs provides a mesoscopically acceptable description of the stem's state.

Our choice of $E_2(M)$ is based on the PBD model which has been widely tested for DNA melting [9,10] but other expressions are certainly possible, provided they properly describe the physics of the molecule. The potential between the bases has to include a strong repulsion when the bases approach each other ($y_m < 0$) and the force has to tend to zero (constant potential) at large y_m . The Morse potential has the proper qualitative shape. Similarly expressing $W(y_m, y_{m-1})$ by a harmonic interaction with an effective coupling constant $K \exp[-\zeta(y_m + y_{m-1})]$ is a simple way to describe the decay of the stacking which is expected when base pairs open. Studies of variants of the PDB model show that different expressions preserving the same qualitative properties imposed by the physical constraints lead to quantitative changes in the results which are also obtainable - within the accuracy of experimental observations - by varying the PDB model parameters.

It should be noted that expression (3) imposes a priori the bases which can be linked by a pairing potential. In other words it assumes that the base sequences in the terminal regions of the strand are such as to guarantee full pairing in the closed hairpin. Mismatches are thus not allowed in the model. We do not expect them to play a significant role in the physical system, at least in the case of the short stems under consideration, since the relative energetic cost of a mismatched configuration would be high.

The potential energy of the hairpin is $E = E_1(N) + E_2(M)$.

3 Thermodynamic properties

3.1 Constrained partition function and free energy: principle of the derivation.

The fluorescence of DNA beacons is determined by the distance ρ_1 between the two ends of a strand, which carry the fluorophore and the quencher. In order to analyze the experiments we must therefore determine the probability $\mathcal{P}_N(\rho_1)d\rho_1$ that a strand will have an end-to-end distance in the interval $(\rho_1, \rho_1 + d\rho_1)$; this is - within a normalization factor - identical to the constrained configuration partition function

$$\mathcal{Z}_N(\rho_1) = \int \prod_N d\Gamma_N \delta \left(\left| \ell \sum_{i=1}^N \mathbf{R}_i \right| - \rho_1 \right) e^{-\beta E(\Gamma_N)} \quad (4)$$

obtained by integrating the Boltzmann weight over the configuration variables symbolically denoted by Γ_N for a DNA strand of N monomers under the constraint of fixed end-to-end distance imposed by the Dirac delta function. The normalized probability density function

$$\mathcal{P}_N(\rho_1) = \frac{\mathcal{Z}_N(\rho_1)}{\mathcal{Z}_N^0} \quad , \quad (5)$$

is obtained by dividing (4) by the unconstrained partition function

$$\mathcal{Z}_N^0 = \int \prod_N d\Gamma_N e^{-\beta E(\Gamma_N)} \quad . \quad (6)$$

The calculation of $\mathcal{Z}(\rho_1)$ for a hairpin is complicated by the presence of interactions within the stem because they involve the *relative positions* of two segments of the polymer. In order to proceed let us start from the L segments forming the loop. Their study is simpler because they form an ordinary polymer, which, in our case, is described by the KP model. The configuration partition function of the loop is Z_L^0 and the probability that the two ends of the loop are at distance ρ_M , the distance between the two bases at the end of the stem connected to the loop, is

$$P_L(\rho_M) = Z_L(\rho_M)/Z_L^0 \quad . \quad (7)$$

In contrast to the expressions of Eq. (5) which refer to the full hairpin, the corresponding terms in Eq. (7) refer to an ordinary polymer without the additional constraints imposed by the stem. Their derivation is discussed in the subsection 3.2. To stress this distinction we have used a script notation \mathcal{Z}, \mathcal{P} for quantities that cannot be obtained from standard polymer theory.

Now that the loop is characterized, let us derive the partition function of the hairpin by successively adding the segments which form the stem, one segment at a time. If we start from the loop and add one monomer at each

end, we have built one segment of the stem. The distance between the new ends of the strand is now ρ_{M-1} . Using the notation of Eqs. (5) or (7), for this extended polymer consisting of $L + 2$ monomers, we have

$$\mathcal{Z}_{L+2}(\rho_{M-1}) = \mathcal{P}_{L+2}(\rho_{M-1}) \mathcal{Z}_{L+2}^0. \quad (8)$$

In order to evaluate $\mathcal{P}_{L+2}(\rho_{M-1})$, let us introduce a *conditional probability* $S(\rho'|\rho)$ that, if a polymer of p monomers has its ends at distance ρ , a polymer of $p + 2$ monomers, obtained by adding one monomer at each end of the previous one, has the distance ρ' between its ends. For the polymer alone i.e. without the contribution of the energy E_2 in the stem, this conditional probability is such that

$$P_{p+2}(\rho') = \int_0^\infty S(\rho'|\rho) P_p(\rho) d\rho. \quad (9)$$

In the presence of the energy terms E_2 within the stem, the conditional probability $S(\rho'|\rho)$, determined by the properties of the polymer alone, must be corrected by a Boltzmann factor containing the potential energy terms $V(\rho) + W(\rho', \rho)$ due to base pairing and stacking interactions. Accordingly, the hairpin with a single pair of complementary bases will satisfy

$$\mathcal{P}_{L+2}(\rho_{M-1}) = \int_0^\infty d\rho_M e^{-\beta[V(\rho_M) + W(\rho_{M-1}, \rho_M)]} \times S(\rho_{M-1}|\rho_M) P_L(\rho_M). \quad (10)$$

The process can be iterated to add the remaining segments of the stem. The advantage of this progressive buildup of the stem is that it explicitly introduces the distances between the bases that pair in the stem in the calculation, allowing us to include the proper statistical weights arising from pairing and stacking energies in the stem.

Once all the stem segments and stem energy terms have been included we obtain

$$\begin{aligned} \mathcal{Z}_N(\rho_1) = \mathcal{Z}_N^0 & \int d\rho_2 \dots \int d\rho_M e^{-\beta V(\rho_1)} \\ & \times e^{-\beta[V(\rho_2) + W(\rho_1, \rho_2)]} \times \dots \\ & \times e^{-\beta[V(\rho_M) + W(\rho_{M-1}, \rho_M)]} \\ & \times S(\rho_1|\rho_2) \dots S(\rho_{M-1}|\rho_M) \\ & \times P_L(\rho_M). \end{aligned} \quad (11)$$

This expression gives the constrained partition function of the hairpin in terms of properties of the polymer forming the strand, $P_L(\rho)$ and $S(\rho'|\rho)$. It is therefore valid for any polymer model, provided one can derive these two probability distributions for the model of interest. The constrained partition function $\mathcal{Z}_N(\rho_1)$ defines an effective free energy $\mathcal{F}(\rho_1) = -k_B T \ln \mathcal{Z}_N(\rho_1)$ for the hairpin having the distance ρ_1 between its ends, i.e. it gives the free energy landscape using ρ_1 as the relevant coordinate. The result appears as a $(M - 1)$ -dimensional integral but - like any transfer integral - it can actually be computed by a sequence of $M - 1$ one-dimensional integrations. Performing first the integration over ρ_M , we get a function of ρ_{M-1} ;

next, the integration over ρ_{M-1} gives a function of ρ_{M-2} , and so on, until the last integration over ρ_2 which gives the desired constrained partition function. Therefore, the calculation of $\mathcal{Z}_N(\rho_1)$ is a relatively straightforward numerical task since $P_L(\rho)$ and $S(\rho'|\rho)$ can be derived from appropriate polymer models.

3.2 The properties of the Kratky-Porod model, and the effective Gaussian approximation

In order to proceed further with the calculation of $\mathcal{F}(\rho_1)$ we need expressions of $P_L(\rho)$ and $S(\rho'|\rho)$ for the polymer model chosen to describe the DNA strand, i.e. the Kratky Porod (KP) model having an energy given by Eq. (2). This model has been widely studied in the continuum limit, known as wormlike chain (WLC) where the energy tends to

$$E'_1 = \frac{\kappa}{2} \int_0^\Lambda dx \left| \frac{\partial \mathbf{R}}{\partial x} \right|^2 \quad (12)$$

for a given chain length $\Lambda = L\ell$, in the limit $L \rightarrow \infty$, $\ell \rightarrow 0$, provided $\epsilon\ell^3 \rightarrow \kappa$, the continuum chain stiffness.

However, the probability distribution function $P(\rho)$ obtained in the continuum limit [12,13,14,15] is not appropriate for DNA hairpins for which the loops may not be longer than a few persistence lengths of single-stranded DNA and the persistence length itself hardly exceeds the monomer distance. In this case the continuum limit becomes a priori questionable and the discrete expression of Eq. (2) should be preserved. The partition function \mathcal{Z}_L^0 of a polymer of L segments is readily calculated as

$$\mathcal{Z}_L^0 = \int d\Omega_1 \dots d\Omega_L e^{-\beta E_1(L)} = 4\pi [4\pi e^{-b} i_0(b)]^{L-1}, \quad (13)$$

where $b = \beta\epsilon\ell^2$ and $i_0(b) = \sinh(b)/b$ is the modified Bessel function of zeroth order. The mathematical equivalence of this model with the classical Heisenberg ferromagnetic chain [16] can be used to show that the orientational correlations between different segments have the form

$$\langle \mathbf{R}_r \cdot \mathbf{R}_s \rangle = e^{-|r-s|\ell/\lambda}, \quad (14)$$

with a persistence length

$$\lambda = -\frac{\ell}{\ln[i_1(b)/i_0(b)]} = -\frac{\ell}{\ln[\coth(b) - 1/b]}, \quad (15)$$

where $i_1(b) = [b \cosh(b) - \sinh(b)]/b^2$ is the modified Bessel function of first order. For the discrete KP model, the end-to-end distribution function can be computed numerically from its Fourier transform, which can be expressed [17] as the leading matrix element

$$P_N^{KP}(\mathbf{q}) = (\mathbf{F}^N)_{00} \quad (16)$$

of the N th power of a symmetric matrix \mathbf{F} whose elements are given by

$$F_{l'l'}(q) = \frac{1}{2} \left[(2l+1)(2l'+1) \hat{i}_l(b) \hat{i}_{l'}(b) \right]^{1/2} \sum_{k=|l-l'|, k+l+l'=2r}^{l+l'} (2k+1) (-i)^k \frac{1}{r+1/2} \frac{\Psi(r-k) \Psi(r-l) \Psi(r-l')}{\Psi(r)} j_k(q) \quad , \quad (17)$$

where

$$\Psi(n) = \frac{\Gamma(n + \frac{1}{2})}{\Gamma(n+1)\Gamma(\frac{1}{2})} = \prod_{j=1}^n \left(1 - \frac{1}{2j} \right) \quad ,$$

$j_k(q)$ is the spherical Bessel function of k th order, and $\hat{i}_l(b) = i_l(b)/i_0(b)$. In practice one can obtain numerically accurate results even for short stiff polymers ($L = 10$, $\lambda = 0.8L\ell$ for instance) by summing no more than 8 terms in (17). Furthermore, since only the leading matrix element is required, direct matrix multiplication is quite efficient.

The derivation of the conditional probability $S(\rho'|\rho)$ is even more demanding than the calculation of $P(\rho)$ and we have not been able to obtain it for the KP model. Fortunately however, in the case of weak chain rigidity, there is a way to go around this difficulty because, as shown in appendix A, the conditional probability $S(\rho'|\rho)$ can be calculated exactly for a Gaussian chain, made of orientationally uncorrelated links such that the probability for any segment to lie along a vector Δ is proportional to $\exp(-|\Delta|^2/4\tau^2)$. It is given by

$$S(\rho'|\rho) = \sqrt{\frac{1}{2\pi\tau^2}} \frac{\rho'}{\rho} e^{-(\rho'^2 + \rho^2)/8\tau^2} \sinh\left(\frac{\rho'\rho}{4\tau^2}\right) \quad . \quad (18)$$

The Gaussian probability function $P^G(\rho)$ can be used to approximate the end-to-end distribution function of the KP chain $P^{KP}(\rho)$ by choosing a temperature dependent value of its parameter $\sigma^2 = L\tau^2$ so that the average square of the end-to-end distance of a Gaussian chain with L segments $\langle \rho^2 \rangle = L\ell^2 = 6\sigma^2 = 6L\tau^2$ matches the average value of $\langle \rho^2 \rangle$ for the KP chain

$$\langle \rho^2 \rangle = L\chi \quad (19)$$

with

$$\chi = \ell^2 \frac{1 + \coth(b) - 1/b}{1 - \coth(b) + 1/b} \quad . \quad (20)$$

To get a Gaussian approximation for the KP chain we must therefore select

$$\tau^2 = \frac{\chi}{6} \quad , \quad (21)$$

Figure 2 shows that the Gaussian approximation is fairly good for $L = 24$ and becomes poor for $L = 14$. However we do not actually need to use $P^G(\rho)$. The advantage of the Gaussian approximation is that it provides the

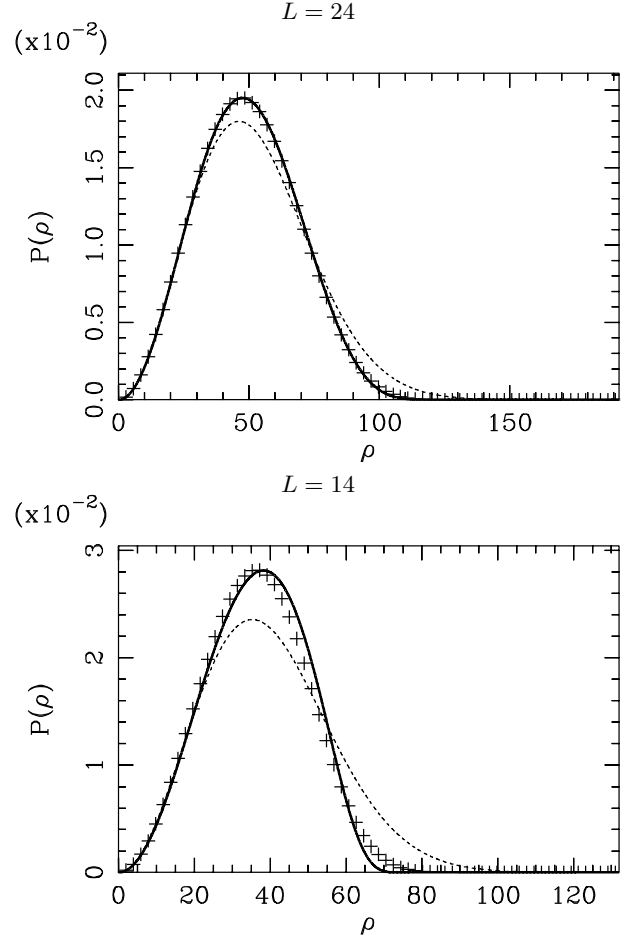


Fig. 2. Comparison between the Kratky Porod distribution function $P_L^{KP}(\rho)$ (full line) and the Gaussian approximation $P_L^G(\rho)$ (dashed line) for two values of L . The crosses show the distribution function $P_L(\rho)$ obtained by starting from the Kratky Porod distribution $P_{L-2}^{KP}(\rho)$ and computing the probability distribution of the end-to-end distance of a polymer extended by two units, using the conditional probability $S(\rho'|\rho)$ according to Eq. 9. The parameters for the KP model are $\epsilon = 0.0016$ eV/Å², $\ell = 6$ Å, and the calculation has been made for $T = 300$ K, giving $b = \beta\epsilon\ell^2 = 2.26$ and $\lambda = 10.8$ Å.

basis for an approximate expression of $S(\rho'|\rho)$ given by Eqs. (18) and (21), which can be used in order to compute P_{L+2} from P_L , according to Eq. (10), by providing for P_L the numerical result $P_L^{KP}(\rho)$, i.e. a value which is very accurate. In this approach the error introduced by the Gaussian approximation only affects the *variation* of $P(\rho)$ when the polymer is extended. Figure 2 shows that, even for a short loop $L = 14$, for which the Gaussian approximation is poor, the comparison between the approximated expression of P_{L+2} and the accurate numerical value P_{L+2}^{KP} is quite good, and becomes excellent for longer loops ($L = 24$). This gives us all the ingredients that we need to compute the constrained partition function of the hairpin $Z_N(\rho_1)$ according to Eq. (11).

3.3 First results.

Before discussing all the results in Sec. 5 it is useful to consider an example which illustrates the thermal properties of hairpins and introduces some quantities which will turn out to be relevant in the next section on kinetic properties.

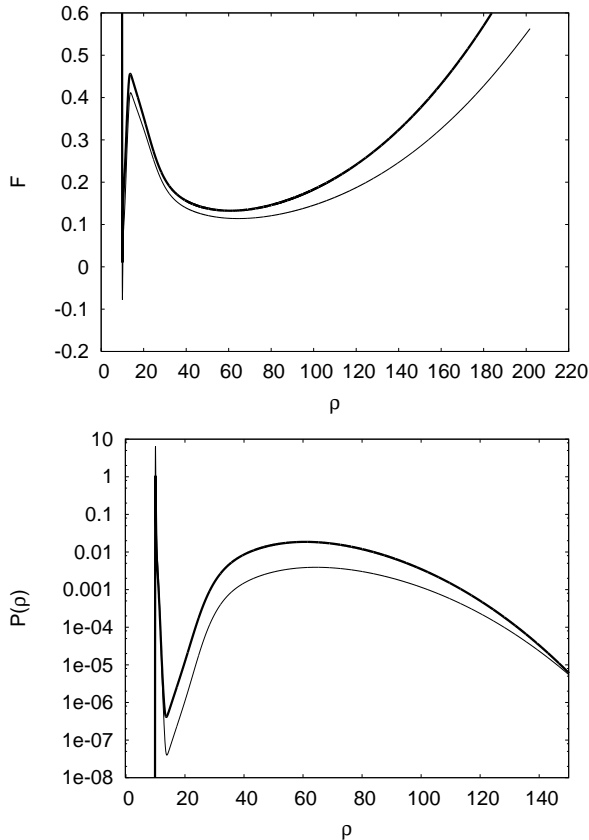


Fig. 3. Behavior of the hairpin model at two different temperatures, $T = 300$ K (thin line) and $T = 350$ K (thick line), for $L = 24$. Top figure: free energy versus ρ_1 , bottom figure: probability density $P(\rho_1)$ in logarithmic scale. The parameters of the model are $D = 0.16$ eV, $\alpha = 6.9 \text{ \AA}^{-1}$, $K = 0.125 \text{ eV/\AA}^2$, $\zeta = 0.10 \text{ \AA}^{-1}$, $\epsilon = 0.0016 \text{ eV/\AA}^2$, $\ell = 6 \text{ \AA}$.

Figure 3 shows the effective free energy $\mathcal{F}(\rho_1)$ for a hairpin with $M = 5$ base pairs in the stem and $L = 24$ segments in the loop, at 300 K and 350 K, and the corresponding probability distributions $\mathcal{P}_N(\rho_1)$. As shown below, these two temperatures are on both sides of the opening temperature T_m of this hairpin. However Fig. 3 shows that $\mathcal{F}(\rho_1)$ and $\mathcal{P}_N(\rho_1)$ maintain the same qualitative shape at both temperatures. $\mathcal{F}(\rho_1)$ has a narrow well around $\rho_1 = 10 \text{ \AA}$ which is the equilibrium distance between the bases in a DNA double helix; the narrow well is separated from a broad secondary minimum at larger ρ_1 by a fairly sharp maximum. The probability density $\mathcal{P}_N(\rho_1) = \mathcal{Z}_N(\rho_1)/\mathcal{Z}_N^0 = \exp[-\beta\mathcal{F}(\rho_1)]/\mathcal{Z}_N^0$ exhibits two peaks. The peak around $\rho_1 = 10 \text{ \AA}$ corresponds to the

closed state of the hairpin, while the broad maximum at large ρ_1 corresponds to the open configurations. This shape of $\mathcal{P}_N(\rho_1)$ points out that, at any temperature, the open and closed forms of the hairpin coexist. The opening “transition” is only a shift of the equilibrium from one temperature regime where the closed configurations dominate to another where the open states are the majority. This is not surprising since even an approximate phase transition should not be expected in a small system such as a DNA hairpin. Therefore, in order to provide a measure of the opening of the hairpin we have to compute the *fraction of open states*, which can be obtained from the probability distribution $\mathcal{P}_N(\rho_1)$ by defining as closed the states for which $\rho_1 \leq \rho^*$ and open those for which $\rho^* < \rho_1 < \rho_{\max}$, where ρ^* is the value of ρ_1 corresponding to the minimum of $\mathcal{P}_N(\rho_1)$ (i.e. the maximum of $\mathcal{F}(\rho_1)$) and $\rho_{\max} = N\ell$ is the maximum distance between the ends of the DNA strand, determined by the length of the strand. The respective probabilities to find the hairpin in the closed and open configurations are thus

$$p_c = \int_0^{\rho^*} \mathcal{P}_N(\rho_1) d\rho_1 \quad p_o = \int_{\rho^*}^{\rho_{\max}} \mathcal{P}_N(\rho_1) d\rho_1. \quad (22)$$

Since $\mathcal{P}_N(\rho_1)$ is normalized, i.e. $p_c + p_o = 1$, p_o also represents the fraction of open configurations at a given temperature. Performing such a calculation as a function of temperature gives the so-called “melting curve” of the DNA hairpin. Figure 4 shows two examples of such curves for $L = 24$ (the case illustrated in Fig. 3) and a case with a shorter loop ($L = 14$). If we define T_m as the temperature at which $p_o = p_c$, we get $T_m(L = 24) = 317.7$ K and $T_m(L = 14) = 337.0$ K for the model parameters that we used in these calculations. In the context of this paper we will also refer to T_m as the opening temperature of the hairpin.

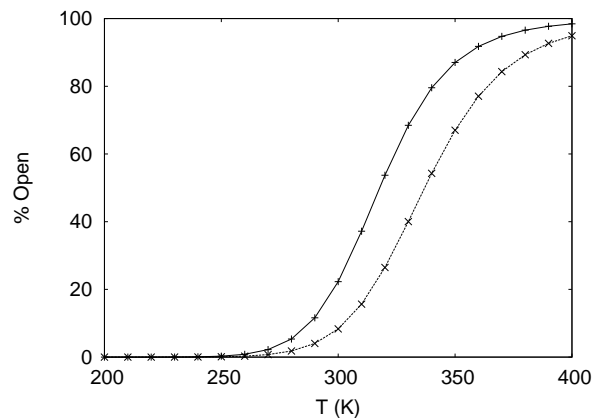


Fig. 4. Variation versus temperature of the percentage of open hairpins for two different loop lengths $L = 24$ (full line) and $L = 14$ (dotted line). The parameters of the model are $M = 5$, $D = 0.16$ eV, $\alpha = 6.9 \text{ \AA}^{-1}$, $K = 0.125$, $\zeta = 0.10 \text{ \AA}^{-1}$, $\epsilon = 0.0016 \text{ eV/\AA}^2$, $\ell = 6 \text{ \AA}$.

4 Kinetics

The derivation of the free energy $\mathcal{F}(\rho_1)$ allows us to go beyond the analysis of the equilibrium properties of the hairpins because it exhibits the characteristic shape of a system evolving between 3 states $C \rightleftharpoons T^* \rightleftharpoons O$, the closed C and open O states associated, respectively, with the minima of $\mathcal{F}(\rho_1)$ and an unstable transition state T^* corresponding to the intermediate maximum. This suggests that the multidimensional dynamics of the opening and closing of the hairpins can be viewed as a reduced problem of reaction kinetics. If the system is strongly coupled to its environment, the dynamics of the molecule has no memory of its velocity so that it is well described by a diffusion on the free energy surface $\mathcal{F}(\rho_1)$. For the large molecular units involved in the opening/closing of DNA hairpins this is a reasonable assumption. Studying the kinetics of hairpin fluctuations is thus reduced to the calculation of a first passage time in a diffusion controlled process [18, 19].

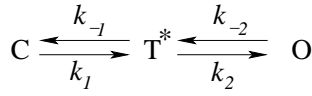


Fig. 5. Schematic of the reaction kinetics view of the hairpin opening/closing, and definition of the reaction rate constants of the processes involved.

In the language of chemical reaction kinetics, if we denote the concentrations in the three states by p_c , p^* , p_o , respectively, and use the kinetic constants defined in Fig. 5, the temporal evolution of the reactants is described by

$$\frac{dp_c}{dt} = -k_1 p_c + k_{-1} p^* \quad (23)$$

$$\frac{dp_o}{dt} = k_2 p^* - k_{-2} p_o \quad (24)$$

$$\frac{dp^*}{dt} = k_1 p_c + k_{-2} p_o - (k_{-1} + k_2) p^* \quad (25)$$

Under the standard assumption of rapid intermediate state dynamics, there is no variation of the concentration p^* on the time scale of the diffusive motion which controls barrier crossing. The condition $dp^*/dt = 0$ implies

$$p^* = \frac{k_1 p_c + k_{-2} p_o}{k_{-1} + k_2} \quad (26)$$

and allows us to eliminate the concentration of the transition state from the equations, leading to

$$\frac{dp_c}{dt} = -\frac{k_1 k_2}{k_{-1} + k_2} p_c + \frac{k_{-1} k_{-2}}{k_{-1} + k_2} p_o \equiv -k_f p_c + k_r p_o \quad (27)$$

$$\frac{dp_o}{dt} = -\frac{k_{-1} k_{-2}}{k_{-1} + k_2} p_o + \frac{k_1 k_2}{k_{-1} + k_2} p_c \equiv -k_r p_o + k_f p_c \quad (28)$$

The equilibrium concentrations \bar{p}_c and \bar{p}_o satisfy the relationship $\bar{p}_c/\bar{p}_o = k_r/k_f$, which allows us to rewrite the inverse of the forward and reverse kinetic constants as

$$k_f^{-1} = k_1^{-1} + \frac{\bar{p}_c}{\bar{p}_o} k_{-2}^{-1} \quad (29)$$

$$k_r^{-1} = k_{-2}^{-1} + \frac{\bar{p}_o}{\bar{p}_c} k_1^{-1} \quad (30)$$

The ratio of equilibrium concentrations is given by the ratio of partition functions of the corresponding states

$$\frac{\bar{p}_c}{\bar{p}_o} = \frac{\mathcal{Z}_c}{\mathcal{Z}_o}, \quad (31)$$

where \mathcal{Z}_c and \mathcal{Z}_o designate the partition function of the hairpin restricted to $\rho_1 < \rho^*$ or $\rho_1 > \rho^*$ respectively. The kinetic parameters are now expressed only in terms of equilibrium properties and the lifetimes k_1^{-1} and k_{-2}^{-1} of the closed and open states, which we must evaluate.

Each of the two states corresponds to a basin of the free energy $\mathcal{F}(\rho_1)$, and the lifetime of the closed and open states is therefore the first passage time of the coordinate ρ_1 above the barrier that defines the boundary between the two basins for $\rho_1 = \rho^*$. The diffusion on the free energy surface is described by the Smoluchowski equation

$$\frac{\partial \mathcal{P}(\rho_1, t)}{\partial t} = -\frac{\partial j(\rho_1, t)}{\partial \rho_1} \quad (32)$$

$$j(\rho_1, t) = -D_0 \left[\frac{\partial \mathcal{P}(\rho_1, t)}{\partial \rho_1} + \beta \frac{\partial \mathcal{F}(\rho_1)}{\partial \rho_1} \mathcal{P}(\rho_1, t) \right], \quad (33)$$

where $j(\rho_1, t)$ is the current of the probability $\mathcal{P}(\rho_1, t)$ that the distance between the ends of the hairpin is ρ_1 at time t .

The diffusion coefficient D_0 is determined by the actual diffusive mechanism of the elements of the DNA strand in the solvent that surrounds the hairpin. It could in principle depend on ρ_1 , but a reasonable assumption in an ordinary solvent is to consider D_0 as a constant. Its value sets the timescale of the opening/closing of the hairpin.

The calculation of the first passage time τ for Eq. (33) has been made by Szabo et al. [19]; an alternative derivation, outlined in Appendix B for the sake of completeness, has been given by Deutsch [20]. The result is

$$\tau = \int_{\rho_0}^{\rho^*} dr \frac{1}{D_0 p_0(r)} I^2(r), \quad (34)$$

with

$$I(r) = \int_{\rho_0}^r d\rho p_0(\rho), \quad (35)$$

where ρ_0 defines the limit of the basin of interest ($\rho_0 = 0$ for the basin corresponding to closed hairpins, $\rho_0 = \rho_{\max}$ for open hairpins) and $p_0(r)$ is the probability that $\rho_1 = r$ in the basin of interest, determined by the free energy $\mathcal{F}(\rho_1)$ according to

$$p_0(r) = \frac{e^{-\beta \mathcal{F}(r)}}{\int_{\rho_0}^{\rho^*} d\rho e^{-\beta \mathcal{F}(\rho)}} \quad (36)$$

From Eq. (29) we get

$$k_f^{-1} = \int_0^{\rho^*} dr \frac{1}{D_0 \exp[-\beta\mathcal{F}(r)]/\mathcal{Z}_c} I_c^2(r) + \frac{\mathcal{Z}_c}{\mathcal{Z}_o} \int_{\rho^*}^{\rho_{\max}} dr \frac{1}{D_0 \exp[-\beta\mathcal{F}(r)]/\mathcal{Z}_o} I_o^2(r), \quad (37)$$

where we denoted by $I_c(r)$ and $I_o(r)$ the integral (35) computed in the basin for closed or open states respectively. To avoid overflows in the calculations it is convenient to rewrite those integrals by introducing inside them the factor $\exp[\beta\mathcal{F}(r)]$. If we define

$$J(r) = \frac{1}{\mathcal{Z}_c} \int_0^r d\rho e^{-\beta[\mathcal{F}(\rho) - \mathcal{F}(r)]} \quad \text{for } r < \rho^* \quad (38)$$

$$J(r) = \frac{1}{\mathcal{Z}_o} \int_r^{\rho_{\max}} d\rho e^{-\beta[\mathcal{F}(\rho) - \mathcal{F}(r)]} \quad \text{for } r > \rho^*, \quad (39)$$

equation (37) gives

$$k_f^{-1} = \mathcal{Z}_c \int_0^{\rho_{\max}} dr \frac{1}{D_0} e^{-\beta\mathcal{F}(r)} J^2(r), \quad (40)$$

and an equivalent expression for k_r^{-1} with \mathcal{Z}_o can also be obtained.

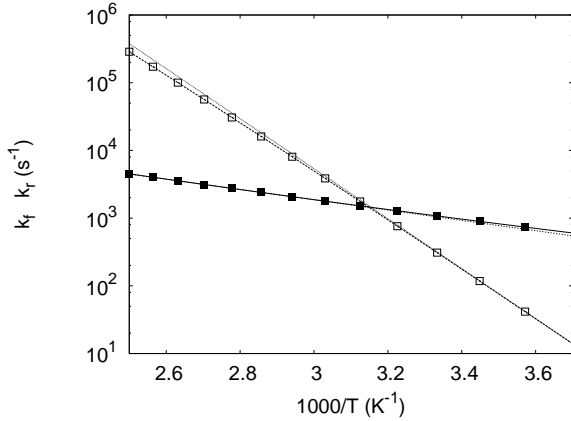


Fig. 6. Opening (open squares) and closing (closed squares) reaction rates k_f and k_r , in logarithmic scale, versus $1000/T$. $L = 24$. The other model parameters are the same as for Fig. 4. The calculation has been made with $D_0 = 3.0 \cdot 10^6$ cm²/s. The full lines show fits by Arrhenius laws with $E_o = 0.73$ eV and $E_c = 0.15$ eV.

Figure 6 shows the temperature dependence of the opening and closing times, k_f^{-1} and k_r^{-1} respectively. The values are proportional to D_0^{-1} , the inverse of the diffusion coefficient introduced in the Smoluchowski equation (33). Measurements for single strands of DNA [21] give diffusion coefficients of $1.5 \cdot 10^6$ cm²/s. We have used the value $D_0 = 3.0 \cdot 10^6$ cm²/s, which is a reasonable estimate for the shorter pieces of DNA strands involved in the closing of the hairpins that we consider. This choice leads to time

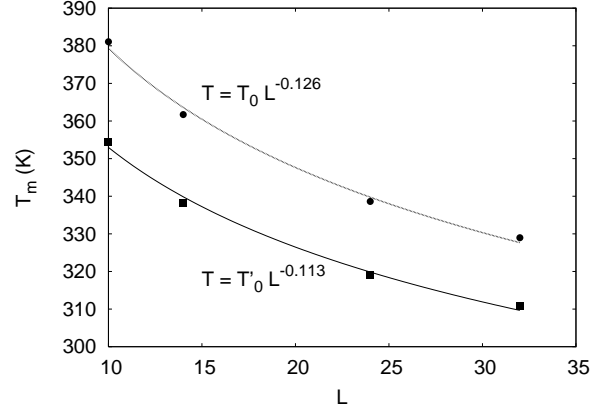


Fig. 7. Variation of the opening temperatures of DNA hairpins deduced from the model where the loop is described by a Kratky Porod model for $\epsilon = 0.0012$ eV/Å² (circles) and $\epsilon = 0.0016$ eV/Å² (squares). The curves show fits with the function $T = T_0 L^\nu$.

scales of k_f^{-1} and k_r^{-1} which are in good agreement with the experiments [6].

Their temperature dependence is well fitted by Arrhenius laws

$$k_f^{-1} \propto e^{\beta E_o} \quad k_r^{-1} \propto e^{\beta E_c}. \quad (41)$$

Both activation energies are positive in agreement with the experimental observations [6]. The opening activation energy $E_o = 0.74$ eV is very close to $MD = 0.80$ eV which is the energy corresponding to the breaking of the M base pairs of the stem.

5 Discussion, role of the model of the loop.

The properties of the model can be examined in the light of experimental studies of DNA beacons which investigated the effect of the length and composition of the loop [6, 22].

Figure 7 shows the variation of the opening temperature T_m versus the length of the loop for two values of the parameter ϵ that governs the rigidity of the Kratky Porod model, $\epsilon = 0.0016$ eV/Å² giving a persistence length $\lambda = 10.82$ Å at 300 K ($\lambda/\ell = 1.8$) and $\epsilon = 0.0012$ eV/Å² giving a persistence length $\lambda = 8.05$ Å at 300 K ($\lambda/\ell = 1.34$). Measurements of the persistence length for single-stranded poly(T) DNA give values in the range 7.5 to 13 Å, depending on the salt conditions, with some measurements leading to values as high as 40 Å [23, 24]. Single-stranded poly(A) can be expected to have a larger persistence length because adenine bases are larger than thymines. However, for short loops it may be difficult to draw a definite conclusion because some all-atom molecular dynamics simulations [25] show that the larger bases may be expelled from the inside of the loop due to steric repulsions while the smaller ones may stay inside and stack on

each other. Paradoxically this could lead to a larger flexibility for a poly(A) loop than for a poly(T). This points out the difficulty to get reliable values of the persistence length from experiments that do not investigate the hairpins themselves. However the values of ϵ that we have selected are in the expected range for single-stranded DNA, and we assume that the larger value of ϵ corresponds to poly(A). Figure 7 shows that, for a given loop length, T_m decreases when the rigidity of the loop increases, in agreement with experiments [22]. Moreover, as observed experimentally, the melting temperature of the hairpins decreases with increasing loop length. For the model we obtain $T_m \propto L^{-\nu}$ with $\nu \approx 0.12$.

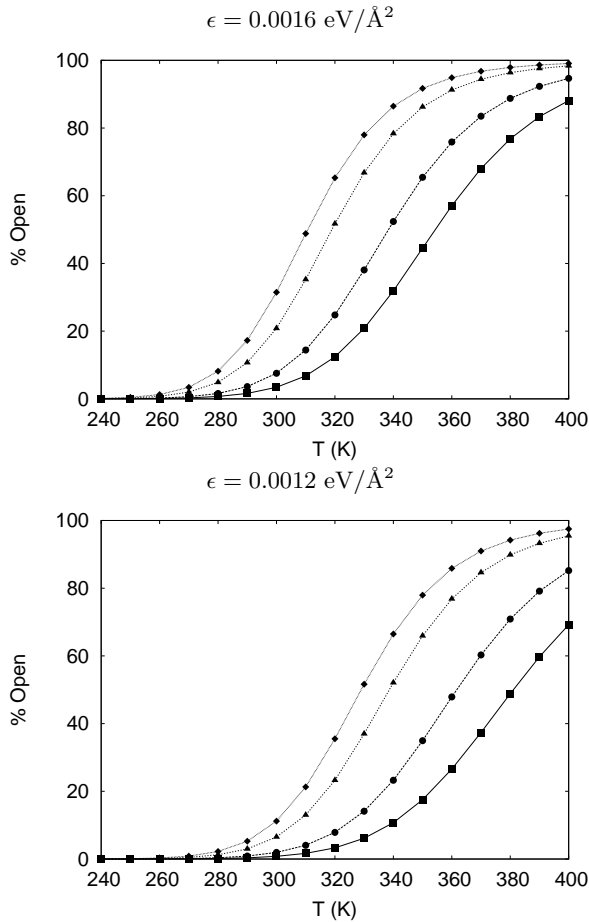


Fig. 8. Variation versus temperature of the percentage of open hairpins for two values of ϵ and different loop lengths: $L = 10$ (squares) $L = 14$ (circles), $L = 24$ (triangles) and $L = 32$ (diamonds).

There are however two aspects on which the model quantitatively disagrees with experiments. First it gives a width of the melting transition which is significantly larger than in experiments. The model finds that the temperature range over which the percentage of open hairpins varies from 20% to 80% extends above approximately 50 K (depending on L) while experiments measure a range of about 15 K for poly(T) loops and about 30 K for

poly(A). Second, as shown in Fig. 8, the model gives a variation of T_m versus L which is approximately the same for poly(A) ($\epsilon = 0.0016$ eV/Å²) and for poly(T) ($\epsilon = 0.0012$ eV/Å²), while experiments indicate that the effect of the loop length L should be significantly larger for poly(A) than for poly(T).

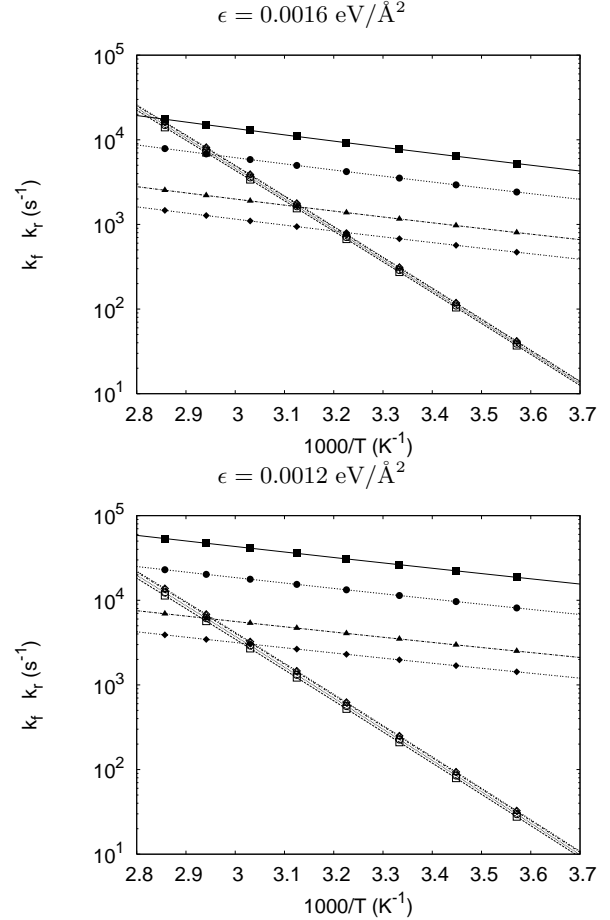


Fig. 9. Variation versus temperature of the reaction rates for opening k_f (open symbols) and for closing k_r (closed symbols) for two values of ϵ and different loop lengths: $L = 10$ (squares) $L = 14$ (circles), $L = 24$ (triangles) and $L = 32$ (diamonds). The reaction rates are plotted in logarithmic scale, versus $1000/T$. The calculations have been made with $D_0 = 3.0 \cdot 10^6$ cm²/s.

Figure 9 shows the variation versus T of the reaction rates for opening k_f and closing k_r for different loop lengths, for two values of ϵ describing poly(A) and poly(T) loops. As noted in subsection 3.3, the order of magnitude of the values that we obtain for the reaction rates are in agreement with the experimental results [6]. Another important point is that k_f is nearly independent of the loop length (Fig. 9) or loop sequence (Fig. 10), as observed experimentally. The variation of k_f versus T is well described by an Arrhenius law with an activation energy $E_o = 0.74$ eV (or 17 kcal/mol, while experiments report a

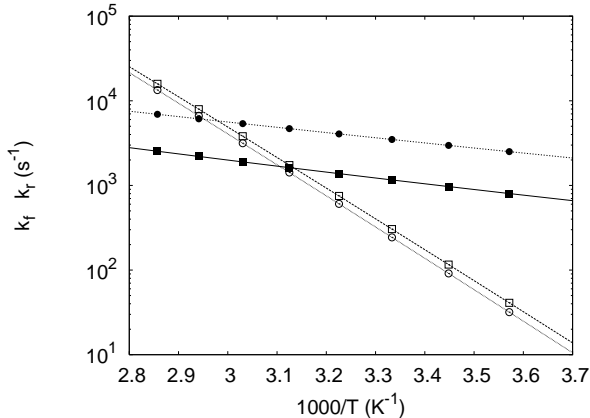


Fig. 10. Comparison of the temperature variation of the reaction rates for opening k_f (open symbols) and for closing k_r (closed symbols) for two values of ϵ : squares $\epsilon = 0.0016 \text{ eV/\AA}^2$ (poly(A)), circles $\epsilon = 0.0012 \text{ eV/\AA}^2$ (poly(T)).

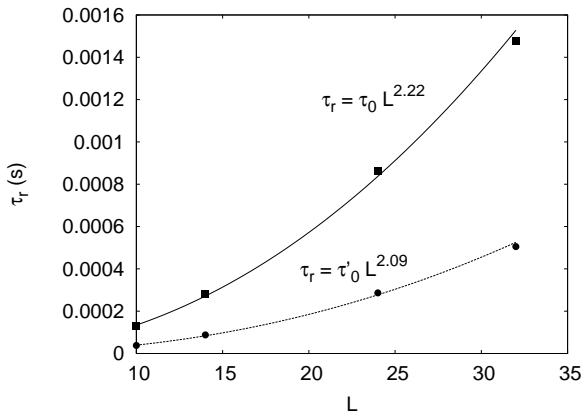


Fig. 11. Closing times of the hairpin at 300 K, $\tau_r = k_r^{-1}$, versus L for two values of ϵ : squares $\epsilon = 0.0016 \text{ eV/\AA}^2$ (poly(A)), circles $\epsilon = 0.0012 \text{ eV/\AA}^2$ (poly(T)). The points are the numerical values given by the model and the lines are fits according to the formula indicated in the graph.

higher value of 34 kcal/mol). Conversely the closing rate depends on the loop length or sequence. Lower rates are obtained for longer, or more rigid, loops, as one would expect qualitatively by considering that closing is mainly determined by the random diffusion of the two sides of the loops that bind when they find each other in space. It is interesting to examine the variation of the closing time $\tau_r = k_r^{-1}$ versus the size of the loop L , shown in Fig. 11. It can be approximated by the scaling law

$$\tau_r = \tau_0 L^\phi \quad (42)$$

with an exponent $\phi = 2.09$ for the poly(T) case and $\phi = 2.22$ for the more rigid poly(A) case. These values should be compared with the values $\phi_0 = 2$ for a Gaussian chain or $\phi_1 = 1.8$ obtained for a flexible polymer with excluded volume effects [26]. Our results that give a lower exponent ϕ when ϵ is reduced are consistent with this theoretical predictions. Some experimental results report an exponent of 2 ± 0.2 [27], but the scaling was measured

on very small loop ($4 \leq L \leq 12$). While the closing rate depends strongly on the loop sequence, in the temperature range that we investigated it is well described by an Arrhenius law with an activation energy that depends weakly on the sequence. For $L = 24$, we get $E_c = 0.148 \text{ eV}$ (3.4 kcal/mol) for $\epsilon = 0.0016 \text{ eV/\AA}^2$ (poly(A)) and $E_c = 0.128 \text{ eV}$ (2.96 kcal/mol) for $\epsilon = 0.0012 \text{ eV/\AA}^2$ (poly(T)).

The results presented up to now have been obtained by describing the DNA strands with a KP polymer model. This model is interesting because it allows us to describe the energetic effects associated to the bending of the strand. However, as we have seen that the results exhibit some limitations of the hairpin model, it is interesting to examine the influence of the model chosen to describe the properties of the loop. Figures 13 to 17 show the results obtained if we consider the strand as a Freely Rotating Chain (FRC) [28], i.e. a polymer made of segments of length ℓ , such that two consecutive segments make a fixed angle θ but can rotate freely around each other (Fig. 12). The energy of a FRC chain is a constant and the contribution of the polymer is only entropic.

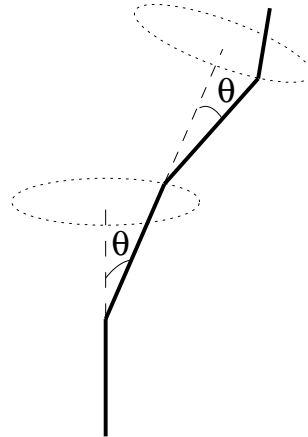


Fig. 12. The Freely Rotating Chain polymer model. The angle between consecutive segments is fixed, and each segment can rotate freely around the axis defined by the previous one.

The probability distribution function $P^{FRC}(\rho)$ of the FRC cannot be expressed analytically but it is easy to obtain it by a Monte Carlo simulation. This numerical expression can be introduced in the calculation of the constrained partition function according to Eq. (11), but, as for the KP chain, we need an analytical expression of $S(\rho'|\rho)$ to carry out the calculations. Figure 13 shows that it can again be provided by an effective Gaussian approximation determined by choosing the parameter τ according to $L\tau^2 = \langle \rho^2 \rangle / 6$. For the FRC, one has $\langle \rho^2 \rangle = L \ell^2 (1 + \cos \theta) / (1 - \cos \theta)$ so that the value of χ to be entered in the expressions (21) and (18) is $\chi = (1 + \cos \theta) / (1 - \cos \theta)$.

In order to compare the two polymer models, we have selected for the FRC case values of θ which give a persistence length comparable to the cases that we investigated

for the Kratky Porod model. The matching cannot be perfect because, as the FRC model has a constant energy, its persistence length does not depend on temperature, contrary to the KP case. We have selected the values of θ so that the persistence length of the two models match at $T = 300$ K. For the FRC model, the persistence length is [28]

$$\lambda' = -\frac{\ell}{\ln(\cos \theta)}. \quad (43)$$

The values $\theta = 54.945^\circ$ and $\theta = 61.667^\circ$ give the same persistence lengths as the KP model at 300 K for $\epsilon = 0.0016$ eV/Å² (poly A) and $\epsilon = 0.0012$ eV/Å² (poly T).

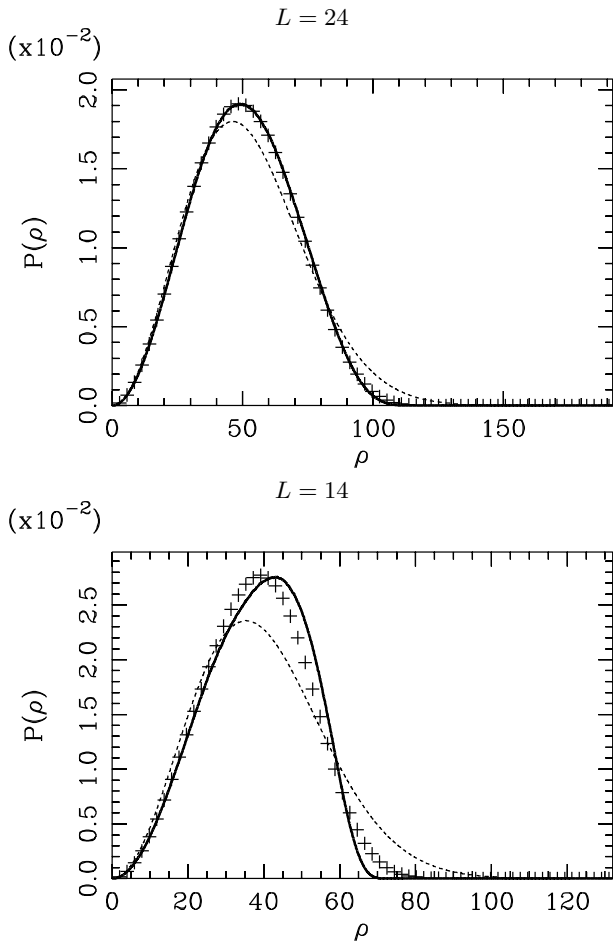


Fig. 13. Comparison between the FRC distribution function $P_L^{FRC}(\rho)$ (full line) and the Gaussian approximation $P_L^G(\rho)$ (dashed line) for two values of L . The crosses show the distribution function $P_L(\rho)$ obtained by starting from the FRC distribution $P_L^{FRC}(\rho)$ and computing the probability distribution of the end-to-end distance of a polymer extended by two units, using the conditional probability $S(\rho'|\rho)$ according to Eq. 9. The parameters for the FRC model are $\theta = 54.945^\circ$, $\ell = 6$ Å, giving a persistence length $\lambda = 10.8$ Å.

The comparison of figures 14 to 17 for the FRC model with the corresponding figures with the KP model shows that most of the results are qualitatively similar for both

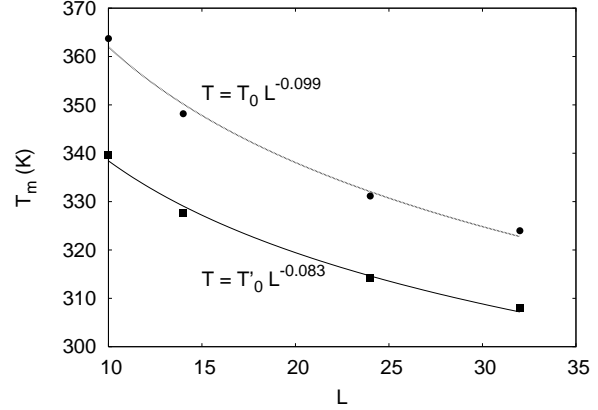


Fig. 14. Variation of the opening temperatures of DNA hairpins deduced from the model where the loop is described by a FRC model for $\theta = 54.945^\circ$ (circles) and $\theta = 61.667^\circ$ (squares). The curves show fits with the function $T = T_0 L^\nu$.

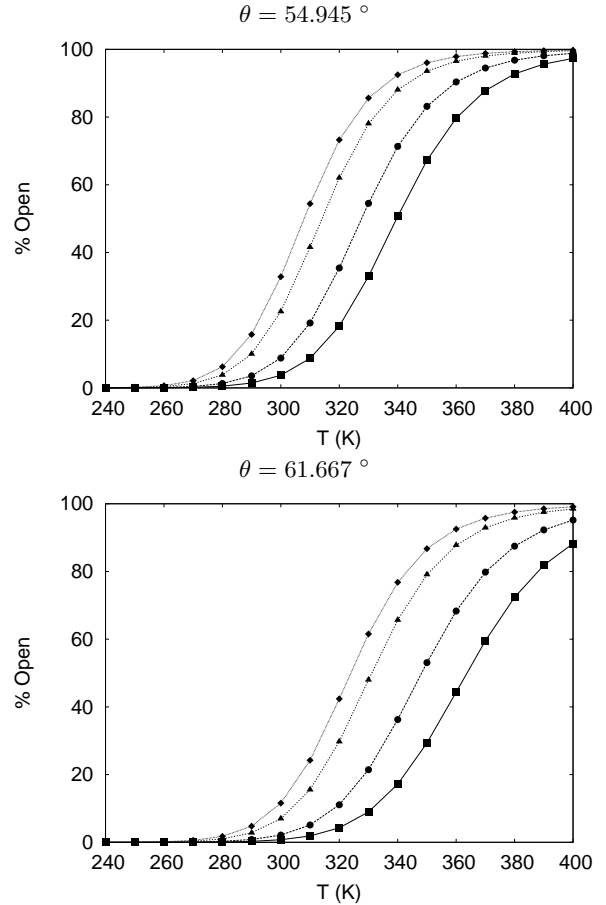


Fig. 15. Variation versus temperature of the percentage of open hairpins with a FRC model of the loop for two values of θ and different loop lengths: $L = 10$ (squares) $L = 14$ (circles), $L = 24$ (triangles) and $L = 32$ (diamonds).

models. The melting curves of Fig. 15 for the FRC model exhibit a narrower temperature range for melting than the corresponding curves of Fig. 8 for the KP model, which

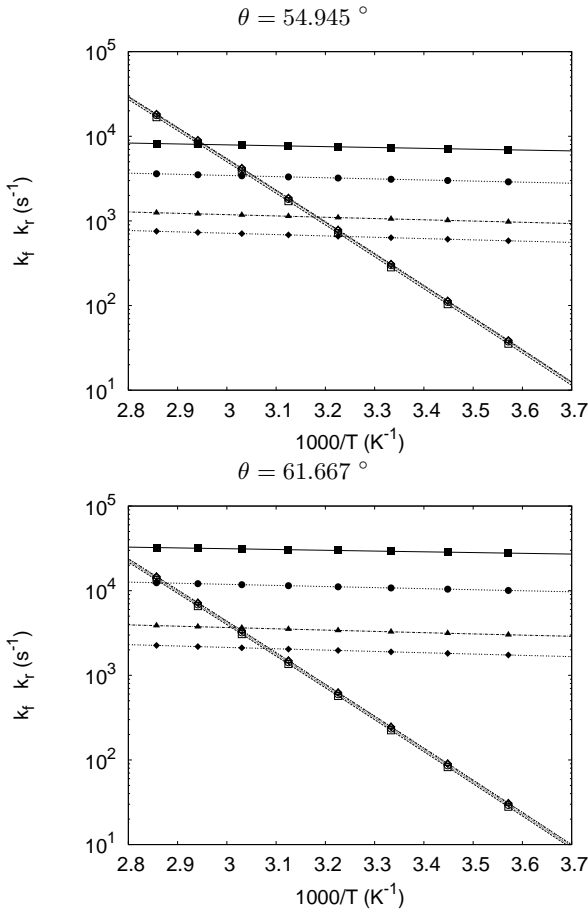


Fig. 16. Variation versus temperature of the reaction rates for opening k_f (open symbols) and for closing k_r (closed symbols) with a FRC model of the loop for two values of θ and different loop lengths: $L = 10$ (squares), $L = 14$ (circles), $L = 24$ (triangles) and $L = 32$ (diamonds). The reaction rates are plotted in logarithmic scale, versus $1000/T$. The calculations have been made with $D_0 = 3.0 \cdot 10^6 \text{ cm}^2/\text{s}$.

would be closer to experimental observations. But both models show a larger variation of T_m when the persistence length of the loop is larger, which disagrees with the observations.

Figures 16 for the FRC model and 9 in the KP case show the same general behavior that the opening rate k_f is almost independent of the length of the loop, whereas the closing rate k_r varies by more than one order of magnitude when L changes from 10 to 32. But there is a qualitative difference between the FRC and Kratky Porod model (which is partly hidden by the logarithmic scales of the figures) concerning the activation energy for closing. While it was of the order of 0.13 eV (3 kcal/mol) for the Kratky Porod model, in agreement with experiments, it is 5 times smaller for the FRC model (≈ 0.57 kcal/mol). This is consistent with the absence of any energy contribution in the FRC, whose rigidity is described in purely geometrical terms, and in fact points out the model's deficiency in describing the properties of DNA strands.

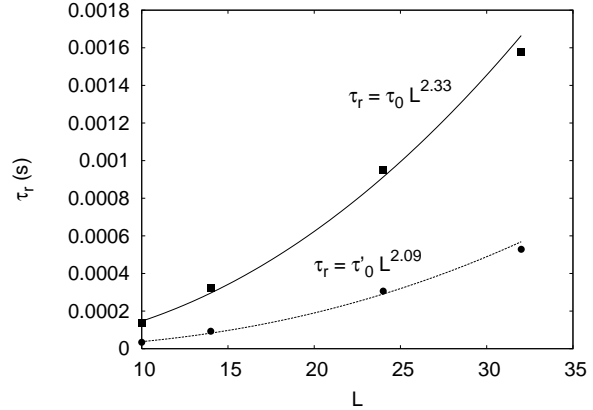


Fig. 17. Closing times of the hairpin at 300 K, $\tau = k_r^{-1}$, versus L for a FRC model of the loop for two values of θ : squares $\theta = 54.945^\circ$ (poly(A)), circles $\theta = 61.667^\circ$ (poly(T)). The points are the numerical values given by the model and the lines are fits according to the formula indicated in the graph.

The effect of the size of the loop on the closing times of the hairpins at 300 K is very similar for the FRC and the KP models (Figs. 17 and 11) because the parameters of the two models have been selected to give the same persistence lengths at this temperature.

In summary, the comparison between alternative descriptions of the polymer properties of DNA single strands shows that different models can bring some quantitative differences but that the qualitative results are not changed; the main discrepancy between theory and experiments concerning the variation of T_m versus L for different loop lengths, which is greater for more rigid loops in experiments while the theory gives the opposite, does not seem to be resolved simply by using another polymer model.

6 Conclusion

In this study we presented a theoretical model of the physics of DNA hairpin formation and melting which tries to capture the essential phenomena within a highly simplified picture. Basically it combines a model for the double helix assembly with standard polymer concepts. This approach exhibits successes and weaknesses which are themselves instructive for understanding the properties of DNA and RNA strands.

Our mesoscopic approach provides acceptable systematics for thermodynamic and kinetic properties of hairpins with a poly(T) loop. Using realistic parameters for the binding energies, persistence length of the loop and diffusion coefficient of the polymer, the KP variant of the model describes the variation of T_m versus L and the order of magnitude of opening and closing times. It shows that the kinetics of the opening is almost unaffected by the length of the loop, in agreement with experiments. Closing times increase very significantly for longer loops while the corresponding activation energy is almost independent of L , as observed experimentally. The enthalpy

of closing is quantitatively described while the enthalpy of opening given by the model is only half of the observed value. This aspect is related to the temperature range over which the melting transition is found in the model, which is significantly broader than in the experiments. Although the model is only semi-quantitative in some respects, it is nevertheless able to describe a whole set of equilibrium and non-equilibrium data with a small set of realistic parameters. It should be stressed that studying thermodynamics *and* kinetics in the same framework is a rather demanding test.

Weaknesses appear when one tries to apply the theory to poly(A) loops. The model correctly detects that T_m is lowered but it finds that the variation of T_m with L is smaller for poly(A) than for poly(T). Intuitively this makes sense because one can understand the decrease of T_m with L as an entropic effect due to the fluctuations of the loop. As poly(A), with its larger bases is considered to be more rigid than poly(T) [22], which is reflected in the higher value of ϵ that we introduce in the KP description of poly(A), one can expect that this extra rigidity reduces fluctuations thereby decreasing the entropy gain due to loop extension. Thus basic physics leads to the conclusion that the effect of the loop length should be smaller for poly(A) than for poly(T) but experiments show exactly the contrary. Another discrepancy between our model and experimental data appears when one examines the enthalpy for closing given by the kinetic studies. Experiments find that ΔH_c is approximately 5 times larger for poly(A) than for poly(T), while we only get a small increase when ϵ is changed from 0.0012 eV/Å² to 0.0016 eV/Å². Varying parameters one can increase ΔH_c for poly(A) in the model, but the disagreement with experiments is transferred elsewhere, in particular on T_m . These discrepancies between theory and experiments for poly(A) are frustrating but probably also very instructive. They suggest that “rigidity” is not the only feature that distinguishes poly(A) from poly(T), otherwise the KP model would be able to describe it. It appears that the effect of having large bases which can stack on each other is deeper and might not be captured by a simple polymer chain model.

In conclusion, attempting to put the thermodynamic and kinetic properties of DNA hairpins in the same model framework remains a challenge. Our results show that the role of the loop is decisive and, for poly(A), extends beyond a simple rigidity effect. This indicates that experiments on hairpins are very sensitive probes of the properties of single-stranded DNA on a scale of a few tens of base pairs. In other words, beacons tell us not only about themselves but also about mesoscopic properties of single-stranded DNA and RNA, which have a high biological relevance.

A Calculation of the conditional probability $S(\rho'|\rho)$ for a Gaussian chain.

Let us consider a Gaussian chain made of orientationally uncorrelated links such that the probability for any segment to lie along a vector Δ is proportional to $\exp(-|\Delta|^2/4\tau^2)$. The probability that the end-to-end distance of a chain of L monomers is at distance ρ is then

$$P^G(\rho) = \frac{1}{2\sqrt{\pi}} \frac{1}{\sigma} \left(\frac{\rho}{\sigma}\right)^2 e^{-\rho^2/4\sigma^2}, \quad (44)$$

with $\sigma^2 = L\tau^2$, where the ρ^2 prefactor comes from the integration over all orientations of the end-to-end vector. It is such that $\langle \rho^2 \rangle = L\ell^2 = 6\sigma^2$. Consider such a Gaussian chain with an end-to-end vector ρ , and assume that we add to each end segments Δ_1 and Δ_2 . Its end-to-end vector becomes $\rho' = \rho + \Delta_1 - \Delta_2$ and the conditional probability that the end-to-end distance of the extended chain is ρ' , given ρ , is

$$S(\rho'|\rho) = A\rho'^2 \int d\Omega_{\rho'} \int d\Delta_1 d\Delta_2 e^{-(\Delta_1^2 + \Delta_2^2)/4\tau^2} \delta(\rho' - \rho - \Delta_1 + \Delta_2) \quad (45)$$

where A is a normalization constant to be determined at the end of the calculation, and where the first integral over the orientations of ρ' is introduced because we are only interested in the end-to-end distance of the chain. The integration over Δ_2 is immediate. Let us define $\mathbf{u} = \rho' - \rho$. Up to a normalization factor we get

$$S(\rho'|\rho) = A\rho'^2 \int d\Omega_{\rho'} \int d\Delta_1 e^{-\Delta_1^2/4\tau^2} \int_{-1}^{+1} d\mu e^{-(\Delta_1^2 + u - 2u\Delta_1\mu)/4\tau^2} \quad (46)$$

where the integral over

$$\mu = \frac{\mathbf{u} \cdot \Delta_1}{u \Delta_1} \quad (47)$$

comes is the integration over the azimuthal angle of Δ_1 . This leads to

$$S(\rho'|\rho) = A\rho'^2 \int d\Omega_{\rho'} \frac{1}{u} e^{-u^2/4\tau^2} \int_0^\infty d\Delta_1 \Delta_1 e^{-\Delta_1^2/4\tau^2} \sinh\left(\frac{u\Delta_1}{2\tau^2}\right) \quad (48)$$

up to normalization factors. Using the definite integral

$$J(a, b) = \int_0^\infty dx x e^{-ax^2} \sinh bx = \frac{b}{4a} \sqrt{\frac{\pi}{a}} e^{b^2/4a}, \quad (49)$$

we can perform the integration over Δ_1 . Reintroducing $\mathbf{u} = \rho' - \rho$, and defining

$$\eta = \frac{\rho' \cdot \rho}{\rho' \rho}, \quad (50)$$

we get

$$S(\rho'|\rho) = A\rho'^2 \int_{-1}^{+1} d\eta e^{-(\rho'^2 + \rho^2 - 2\rho'\rho\eta)/8\tau^2}. \quad (51)$$

Performing the final integration, and determining the normalization constant from

$$\int_0^\infty d\rho' S(\rho'|\rho) = 1 \quad \forall \rho, \quad (52)$$

we obtain

$$S(\rho'|\rho) = \sqrt{\frac{1}{2\pi\tau^2}} \frac{\rho'}{\rho} e^{-(\rho'^2 + \rho^2)/8\tau^2} \sinh\left(\frac{\rho'\rho}{4\tau^2}\right). \quad (53)$$

B Calculation of the first passage time in a diffusion controlled process.

We consider the Smoluchowski equation (33) for the probability distribution $\mathcal{P}(\rho, t)$, with a function $\mathcal{F}(\rho)$ which has the shape of a double well with a local maximum at $\rho = \rho^*$. Initially the system is assumed to be in the well $\rho_0 < \rho < \rho^*$ and we assume a reflecting condition at the boundary $\rho = \rho_0$, which implies $j(\rho_0, t) = 0 \quad \forall t$. To determine the first passage time above the maximum at ρ^* an absorbing boundary condition is assumed for $\rho = \rho^*$. It can be expressed as $j(\rho^*, t) = \kappa\mathcal{P}(\rho^*, t)$ and taking the limit $\kappa \rightarrow \infty$.

The probability that the system is still in the original well at time t is $\int_{\rho_0}^{\rho^*} \mathcal{P}(\rho, t) d\rho$, so that the first passage time above the barrier is

$$\tau = \int_0^\infty dt \int_{\rho_0}^{\rho^*} d\rho \mathcal{P}(\rho, t). \quad (54)$$

and has been calculated in References [19] and [20]. For the sake of completeness we give an outline of the derivation [20] in the context of the present study.

Integrating Eq. (32) with respect to ρ we get an expression of $j(\rho, t)$, which can be used to express the boundary condition at ρ^* as

$$j(\rho^*, t) = \kappa\mathcal{P}(\rho^*, t) = - \int_{\rho_0}^{\rho^*} d\rho \frac{\partial \mathcal{P}(\rho, t)}{\partial t}, \quad (55)$$

and write Eq. (33) as

$$\begin{aligned} \int_{\rho_0}^r d\rho \frac{\partial \mathcal{P}(\rho, t)}{\partial t} &= D_0 \left[\frac{\partial \mathcal{P}}{\partial \rho} + \beta \frac{\partial \mathcal{F}}{\partial \rho} \mathcal{P} \right] \\ &= D_0 e^{-\beta \mathcal{F}} \frac{\partial}{\partial r} [e^{\beta \mathcal{F}} \mathcal{P}] \end{aligned} \quad (56)$$

Integrating over r in the range (R, ρ^*) we get

$$\begin{aligned} e^{\beta \mathcal{F}(\rho^*)} \mathcal{P}(\rho^*, t) - e^{\beta \mathcal{F}(R)} \mathcal{P}(R, t) \\ = \int_R^{\rho^*} \frac{dr}{D_0 e^{-\beta \mathcal{F}(r)}} \int_{\rho_0}^r d\rho \frac{\partial \mathcal{P}(\rho, t)}{\partial t}. \end{aligned} \quad (57)$$

Using the boundary condition (55) we obtain $\mathcal{P}(R, t)$ as

$$\begin{aligned} \mathcal{P}(R, t) &= - \frac{1}{\kappa} \frac{e^{-\beta \mathcal{F}(R)}}{e^{-\beta \mathcal{F}(\rho^*)}} \int_{\rho_0}^{\rho^*} d\rho \frac{\partial \mathcal{P}}{\partial t} - \\ e^{-\beta \mathcal{F}(R)} \int_R^{\rho^*} \frac{dr}{D_0 e^{-\beta \mathcal{F}(r)}} \int_{\rho_0}^r d\rho \frac{\partial \mathcal{P}(\rho, t)}{\partial t} \end{aligned} \quad (58)$$

Let us define $p_0(r)$ by

$$p_0(r) = \frac{e^{-\beta \mathcal{F}(r)}}{\int_{\rho_0}^{\rho^*} d\rho e^{-\beta \mathcal{F}(\rho)}}, \quad (59)$$

which is the probability that the system is at position r in the first well, weighted in this well so that it verifies $\int_{\rho_0}^{\rho^*} p_0(r) dr = 1$. It leads to

$$\begin{aligned} \mathcal{P}(R, t) &= - \frac{1}{\kappa} \frac{p_0(R)}{p_0(\rho^*)} \int_{\rho_0}^{\rho^*} d\rho \frac{\partial \mathcal{P}}{\partial t} \\ &- p_0(R) \int_R^{\rho^*} \frac{dr}{D_0 p_0(r)} \int_{\rho_0}^r d\rho \frac{\partial \mathcal{P}(\rho, t)}{\partial t} \end{aligned} \quad (60)$$

Using this expression to calculate τ according to Eq. (54) gives

$$\begin{aligned} \tau &= \frac{1}{\kappa p_0(\rho^*)} \int_{\rho_0}^{\rho^*} d\rho \mathcal{P}(\rho, t=0) + \\ &\int_{\rho_0}^{\rho^*} dR p_0(R) \int_R^{\rho^*} \frac{dr}{D_0 p_0(r)} \int_{\rho_0}^r d\rho \mathcal{P}(\rho, t=0), \end{aligned}$$

where we used $\lim_{t \rightarrow \infty} \mathcal{P}(\rho, t) = 0 \quad \forall \rho$. Now since the system is assumed to be at equilibrium in the well $\rho_0 < \rho < \rho^*$ at $t = 0$, it follows from the definition of $p_0(\rho)$ that $\mathcal{P}(\rho, t=0) = p_0(\rho)$. Therefore

$$\tau = \frac{1}{\kappa p_0(\rho^*)} + \int_{\rho_0}^{\rho^*} dR p_0(R) \int_R^{\rho^*} \frac{dr}{D_0 p_0(r)} \int_{\rho_0}^r d\rho p_0(\rho), \quad (61)$$

Let us define $H(r)$ by

$$H(r) = \frac{1}{D_0 p_0(r)} \int_{\rho_0}^r d\rho p_0(\rho). \quad (62)$$

We have

$$\begin{aligned} \tau &= \frac{1}{\kappa p_0(\rho^*)} + \int_{\rho_0}^{\rho^*} dR p_0(R) \int_{\rho_0}^{\rho^*} dr H(r) \Theta(r - R) \\ &= \frac{1}{\kappa p_0(\rho^*)} + \int_{\rho_0}^{\rho^*} dr H(r) \int_{\rho_0}^{\rho^*} dR p_0(R) \Theta(r - R) \\ &= \frac{1}{\kappa p_0(\rho^*)} + \int_{\rho_0}^{\rho^*} dr H(r) \int_{\rho_0}^r dR p_0(R) \end{aligned} \quad (63)$$

where $\Theta(x)$ is the Heaviside step function. If we replace $H(r)$ by its expression (62), we obtain

$$\tau = \frac{1}{\kappa p_0(\rho^*)} + \int_{\rho_0}^{\rho^*} dr \frac{1}{D_0 p_0(r)} \left[\int_{\rho_0}^r dR p_0(R) \right]^2 \quad (64)$$

Taking the limit $\kappa \rightarrow \infty$ corresponding to the absorbing boundary condition when the system escapes above the barrier, we finally obtain

$$\tau = \int_{\rho_0}^{\rho^*} dr \frac{1}{D_0 p_0(r)} I^2(r), \quad (65)$$

with

$$I(r) = \int_{\rho_0}^r dR p_0(R), \quad (66)$$

which is the result of Eqs. (34) and (35).

References

1. G. Bonnet and A. Libchaber, *Physica A* **263**, 68 (1999).
2. Xiang-Hong Peng, Ze-Hong Cao, Jin-Tang Xia, G.W. Carlson, M.M. Lewis, W.C. Wood, and L. Yang, *Cancer Res.* **65**, 1909 (2005).
3. P.J. Santangelo, B. Nix, A. Tsourkas and G. Bao, *Nucleic Acid Research* **32**, e57 (2004).
4. M. Takinoue and A. Suyama, *Chem-Bio Informatics Journal* **4**, 93 (2004).
5. K. Sakamoto, H. Gouzu, K. Komiyama, D. Kiga, S. Yokoyama, T. Yokomori and M. Hagiya, *Science* **288**, 1223 (2000).
6. G. Bonnet, O. Krichevsky and A. Libchaber, *Proc. Natl. Acad. Sci. USA*, **95**, 8602 (1998).
7. S.V. Kuznetsov, Y. Shen, A.S. Benight and A. Ansari, *Biophysical J.* **81**, 2864 (2001).
8. O. Kratky and G. Porod, *Recl. Trav. Chim Pays Bas* **68**, 1106 (1949).
9. M. Peyrard, A.R. Bishop *Phys. Rev. Lett.* **62**, 2755 (1989).
10. T. Dauxois, M. Peyrard and A.R. Bishop *Phys. Rev. E* **47**, 684 (1993).
11. Note that the stacking interaction that we use here is different from the expression used in the PBD model $\frac{1}{2}K [1 + \rho \exp[-\zeta(y_m + y_{m-1})]] (y_m - y_{m-1})^2$ because the PBD model does not include an explicit description of the strands, and must not allow a complete vanishing of the interaction, which would mean a breaking of the DNA strand.
12. J. Wilhelm and E. Frey, *Phys. Rev. Lett.* **77**, 2581 (1996).
13. B. Hamprecht and H. Kleinert, *Phys. Rev. E* **71**, 031803 (2005).
14. J. Samuel and S. Sinha, *Phys. Rev. E* **66**, 050801 (2002).
15. S. Stephanow and G.M. Schütz, *Europhys. Lett.* **60**, 546 (2002).
16. M.E. Fisher, *Am. J. Phys.* **32**, 343 (1964).
17. This result has been derived in a slightly different form - which includes the case of an external force - by J. Yan, R. Kawamura and J. Marko, *Phys. Rev. E* **71**, 061905 (2005).
18. K. Schulten, Z. Schulten, and A. Szabo, *J. Chem. Phys.* **74**, 4426 (1981).
19. A. Szabo, K. Schulten and Z. Schulten, *J. Chem. Phys.* **72**, 4350 (1980).
20. J.M. Deutsch, *J. Chem. Phys.* **73**, 4700 (1980).
21. E. Stellwagen and N.C. Stellwagen, *Electrophoresis* **23**, 2794 (2002).
22. N.L. Goddard, G. Bonnet, O. Krichevsky and A. Libchaber, *Phys. Rev. Lett.* **85**, 2400 (2000).
23. S.B. Smith, Y. Cui and C. Bustamante, *Science* **271**, 795 (1996).
24. C. Rivetti, C. Walker and C. Bustamante, *J. Mol. Biol.* **280**, 41 (1998).
25. S. Cuesta López and Y.H. Sanejouand, private communication.
26. P.G. de Gennes, *Scaling concepts in Polymer Physics*. Cornell University Press, N.Y., 1979.
27. A. Ansari, Y. Shen and S.V. Kuznetsov, *Phys. Rev. Lett.* **88**, 069801 (2002).
28. P.J. Flory, *Statistical mechanics of chain molecules*, Interscience, 1969.